A Broadband Low-Profile Circularly Polarized Radial Line Slot Antenna

Matthieu Bertrand, Mauro Ettorre, Guido Valerio, Matteo Albani, M. Casaletti

A Broadband Low-Profile Circularly Polarized Radial Line Slot Antenna

M. Bertrand, M. Ettorre, *Senior Member, IEEE*, G. Valerio, *Senior Member, IEEE,* M. Albani *Fellow, IEEE*, and M. Casaletti, *Senior Member, IEEE*

***Abstract*—This paper presents a circularly polarized Corporate-Fed Radial-Line Slot Antenna (CF-RLSA) operating in Ka-band and realized in low-cost, low-profile printed circuit board (PCB) technology. The radiating aperture is fed by a corporate feed network based on a broadband pillbox-like circular transition. The proposed feeding system results in a 67% gain bandwidth improvement compared to classical center-fed RLSA designs. Pattern stability versus frequency is also achieved. The bandwidth improvement provided by the corporate-feed topology is analytically derived for the general case of circular apertures with uniform amplitude illumination. This predicted improvement is confirmed by measurements. The prototype is optimized using a dedicated numerical tool, then fabricated and characterized. A good agreement is obtained between simulated and measured gain bandwidths, with a demonstrated relative bandwidth of 6.9% at 29 GHz for a maximum gain of 35.5 dBi and a 260 mm diameter for the radiating aperture.**

***Index Terms*—Radial Slot Line Antenna (RLSA), leaky-wave antenna, pillbox, optimization.**

I. Introduction

Recent developments in antenna topologies have focused on the realization of low-profile, low-cost, high efficiency, and high directivity antennas. Different applications drive such developments. For example, the latest 5G communication networks require beam agility as well as wide-band operation in millimeter-wave frequency bands. In the same trend, both military and civil satellite communications demand the integration of high gain, wide-band flat radiating panels for integration on moving platforms such as airplanes and trains. For satellite communications as well as terrestrial links, a circular polarization (CP) is often required for a reliable link in most environmental conditions and location of the users. Straightforward methods for CP radiation are the excitation in phase quadrature of orthogonal radiating elements or placing a polarizer in front of a linearly polarized (LP) radiator. The first solution usually requires a complex feeding network whereas, the latter exhibits design challenges, especially for a wide field of view.

Conversely, several topologies producing a CP radiated field without a complex feeding structure or polarizer have been introduced in the past. In particular, leaky-wave antennas such as slotted waveguides can produce a circularly polarized field by properly positioning slots on the waveguide walls. The radial version of a leaky-wave antenna (RLSA), uses a radially propagating transverse electromagnetic (TEM) in a Parallel Plate Waveguide (PPW) to feed radiating CP slot pairs etched on one of the plates. Such an antenna type was first introduced in the 1960s [1] and later extensively used for Direct Broadcast Satellite (DBS) consumer applications in X-band [2], [3]. Both single layer [2] and double-layer implementations [3] were demonstrated, aiming for high gain broadside radiation with high efficiency and reduced grating lobes. Such antennas were realized in low-loss, heavy metallic PPWs. Since then, a great amount of research has been devoted to the RLSA development.

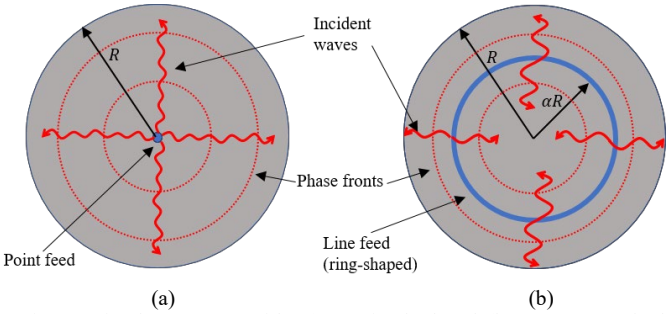

Fig. 1. Circular aperture with (a) a point-feed and (b) a corporate-feed topologies. For a uniform aperture distribution with azimuthal symmetry, the corporate feed takes the shape of a ring.

Adjusting the slot distribution, various polarizations were achieved, such as dual circular [4], linear [5], [6], and dual linear [7]. Research efforts have also been focused on shaping the radiated pattern, obtaining for instance elliptic [8], isoflux [9], conical [10], and tilted beam [11] far-field patterns. Near-field shaping has also been successfully demonstrated [12], [13]. Finally, major progress has also been produced toward

This work was supported in part by the Direction Générale de l'Armement (DGA) through the ANR ASTRID Fast-HEM-3D project.

M. Bertrand was with GeePs CNRS (UMR 8507) Sorbonne Université. He is now with Thales TRT France (e-mail: matthieu-m.bertrand@thalesgroup.com).

M. Casaletti and G. Valerio are with GeePs CNRS (UMR 8507) Sorbonne Université, France (e-mail: massimiliano.casaletti, guido.valerio @sorbonne-universite.fr).

M. Ettorre is with Univ. Rennes, CNRS, IETR (Institut d'Électronique et des Technologies du numéRique) – UMR 6164, 35000 Rennes, France (e-mail: mauro.ettorre@univ-rennes1.fr).

M. Abani is with the Department of Information Engineering and Mathematics (DIISM), University of Siena, Via Roma 56, 53100 Siena, Italy (e-mail: matteo.albani@unisi.it).

modeling [14], [15], design, and optimization-tool development [9], [16].

One of the main limitations of leaky-wave antennas such as the RLSA is bandwidth for a defined pointing direction. Typically, a conventional RLSA gain bandwidth is limited to 3 to 4 percent for realized gains above 35 dBi. Such high gain values can only be realized by large apertures, which naturally suffer from phase error as the frequency strays away from the design frequency. The fundamental reason for that is the large distance between the radiating elements and the center feed point. Current solutions to this problem consist in using low permittivity effective multilayer materials [17] (emulating the vacuum case) or using radially modulated dielectrics[18], [19] to create different radiating regions at different frequencies. This latter solution can achieve large bandwidths at the cost of a low aperture efficiency (maximum 30%).

In 1991, a Japanese patent addressing this specific limitation was filed for a metallic corporate-fed RLSA [20]. The proposed implementation consisted of a combination of H-plane power splitters and waveguide bends to excite the aperture at different locations. According to the authors, this solution could provide a bandwidth increment by at least a factor of 2. While the concept was highly attractive, the realization of such a corporate feed relied on heavy metallic parts with a complex assembly [20], [21]. Recently, technological evolutions such as substrate integrated waveguide (SIW) technology have paved the way for low-cost planar realization of large complex antennas with PCB fabrication processes [22], [23]. Based on these new developments, we present a low-profile, low-cost CF-RLSA operating in Ka-band and achieving a 70% bandwidth improvement as compared to its central-fed RLSA counterpart. The corporate-feed network is based on a novel circular pillbox transition [19] (see Fig. 1). The paper is organized as follows.

In Section II, the upper bound for the antenna bandwidth for a uniform radiating aperture fed by a central point source and the circular corporate-feed network are derived, leading to an estimated theoretical bandwidth improvement factor. The practical implementation, the design procedure, and the optimization of a CF-RLSA in PCB technology is presented in Section III. Section III reports the realized prototype and the comparison between measurements and simulations. Finally, conclusions are drawn in Section IV.

II. Theoretical Investigation of a Line-Fed Uniform Aperture: Bandwidth Enhancement

In this section, we provide a theoretical argumentation for a CF-RLSA and derive an estimated bandwidth improvement factor, as compared to conventional point-fed RLSAs. In particular, we consider the gain degradation related to the increasing phase error on a uniformly illuminated aperture. It is worth mentioning that other factors such as slot polarizability dispersion and edge back-scattering could also impact the gain bandwidth. However, we assume here that such effects may be neglected with respect to the phase error since edge effects can be practically mitigated by using absorbing materials at the antenna's outer edges. First, the gain bandwidth limitation is shown for a conventional point-fed circular aperture. Then, for the same aperture, we demonstrate the estimated bandwidth improvement provided by the integration of a corporate feed network.

A. Bandwidth limitation of point-fed uniform apertures

This section aims to evaluate the variation of directivity as a function of frequency for a uniform aperture. In this derivation, the impact of the aperture sampling provided by the slots in RLSA antennas is not considered. In practice, such a sampling does not impact the radiated far-field if correctly implemented, by small slot spacing compared to the free-space wavelength [9]. Let us, therefore, consider an aperture on a disk of radius R radiating in the upper half-space. The aperture is discretized in several current elements, each of them being illuminated by an outward radial wave propagating in the lower half-space with a wavenumber $k(\omega_0)$, where ω_0 is the operating angular frequency. This corresponds to a feed point placed at the center of the aperture (see Fig. 1(a)). The complex electric-field component radiated by a single current element is written $\mathbf{EF}(\theta,\phi,\omega)$, where (θ,ϕ) denotes the angular spherical coordinates. This current element can represent a single linearly polarized slot, or a pair of slots in quadrature radiating a circular polarization. The total field $\mathbf{E}(\theta,\phi,\omega)$ is thus given by:

$$\mathbf{E}(\theta,\phi,\omega) = AF(\theta,\phi,\omega)\mathbf{EF}(\theta,\phi,\omega) \tag{1}$$

where $AF(\theta,\phi,\omega)$ is the array factor. Let us now assume that the array is designed for the nominal frequency ω_0, such as that all currents are synchronously radiating at broadside at this frequency. If we assume an aperture sampling sufficiently dense and therefore neglect the impact of the sampling, it naturally follows that $AF(\theta,\phi,\omega_0) = \pi R^2$, where R is the aperture radius. At any different frequency $\omega \neq \omega_0$, the aperture is illuminated by a radial wave with wavenumber $k(\omega)$, and the phase distribution presents a linear phase error along the radial direction proportional to the field path from the source to the radiating point (slot). Therefore, the phase shift error is given by $\left[k(\omega)-k(\omega_0)\right]\rho$, where k is the wave vector of this incident wave, so that:

$$AF(0,0,\omega) = \int_0^{2\pi}\int_0^{R} e^{-j\left[k(\omega)-k(\omega_0)\right]\rho}\rho d\rho d\phi\,. \tag{2}$$

Introducing the maximum phase-shift error at the antenna edge $\Delta(\omega) = \left(k(\omega)-k(\omega_0)\right)R$, (2) simplifies as:

$$AF(0,0,\omega) = \frac{2\pi R^2}{\Delta^2(\omega)} e^{-j\Delta(\omega)}\left[j\Delta(\omega)+1-e^{j\Delta(\omega)}\right]. \tag{3}$$

In addition, if we assume that the field radiated by each element is slowly changing around the nominal frequency ω_0, the power density S radiated at broadside can be written as:

$$S(0,0,\omega) = \frac{1}{2\zeta_0}\left|AF(\theta,\phi,\omega)\right|^2\left|\mathbf{EF}(\theta,\phi,\omega)\right|^2. \tag{4}$$

Thus, the power density variation over frequency is given by

$$\frac{S(0,0,\omega)}{S(0,0,\omega_0)}=\frac{\frac{1}{2}\left|AF(\theta,\phi,\omega)\right|^2\left|\mathbf{EF}(\theta,\phi,\omega)\right|^2}{\frac{1}{2}\pi^2R^4\left|\mathbf{EF}(\theta,\phi,\omega_0)\right|^2}\simeq\frac{1}{\pi^2R^4}\left|AF(\theta,\phi,\omega)\right|^2 \tag{5}$$

Finally, using Taylor's first-order approximation with respect to the small parameter Δ, (5) reduces to:

$$\left|AF(0,0,\omega)\right|^2\simeq\pi^2R^4\left\{1-\frac{\Delta^2(\omega)}{18}\right\} \tag{6}$$

Considering a conventional aperture made of slots etched on the top of a PPW with a dielectric constant $\varepsilon_0\varepsilon_r$, the radial wavenumber is $k(\omega)=\omega\sqrt{\varepsilon_r\varepsilon_0\mu_0}$ and the 3-dB frequency bandwidth can then be estimated by equating this ratio to 1/2, leading to the following bounds:

$$\omega_{3dB}^{1,2}=\omega_0\pm3\frac{c_0}{\sqrt{\varepsilon_r}R}, \tag{7}$$

where c_0 is the speed of light in vacuum.

The absolute bandwidth B is thus given by

$$B=\frac{3c_0}{\sqrt{\varepsilon_r}\pi R} \tag{8}$$

These derivations do not take into account several parameters, such as the spatial sampling of the aperture as well as the frequency variations of the field radiated by each current element. However, these secondary elements usually have a small impact on the gain variation at the broadside compared to the phase error appearing immediately on the aperture as the frequency departs from ω_0.

B. Bandwidth improvement offered by a line-fed aperture

In this section, the results presented in II-A are extended to the corporate-feed case. In particular, as shown in Fig. 1(b), it is assumed that the antenna feeder is a ring-shaped line of radius $\rho=\alpha R$, where α is a real positive constant smaller than 1. The practical realization of this feed will be discussed in Section III. To maintain an azimuthally uniform aperture distribution, a constant phase along the circle is assumed. In this condition, the radiating elements placed inside the circle are excited by an inward propagating wave, while the others are excited by an outward propagating one. Finally, it is assumed that all the incoming power is radiated by the antenna so that the inward propagating wave does not reverse itself into an outward one at the antenna center, and the outward propagating wave is not reflected by the antenna edge.

In this context, the element factor and the array factor at the design frequency ω_0 are the same as for the point-fed RLSA. At a general angular frequency ω, the aperture linear phase error in the array factor depends on the distance of a particular source point (slot) from the ring feed, namely

$$AF(0,0,\omega)=\int_0^{2\pi}\int_0^{R}e^{-j\left(k(\omega)-k(\omega_0)\right)\left|\rho-\alpha R\right|}\rho d\rho$$

$$=\frac{2\pi R^2e^{-j\alpha\Delta(\omega)}}{\Delta^2(\omega)}\left[-1+e^{-j\Delta(\omega)(1-2\alpha)}\left(1+j\Delta(\omega)\right)-2j\alpha\Delta(\omega)e^{j\alpha\Delta(\omega)}\right] \tag{9}$$

As done previously, using Taylor's expansions in (9) leads to the simplified equation:

$$\left|AF(0,0,\omega)\right|^2\simeq\pi^2R^4\left\{1+\frac{1}{18}\left(-1+16\alpha^3-24\alpha^4+8\alpha^6\right)\Delta^2(\omega)\right\} \tag{10}$$

Then, it follows that the radiated power density variation around ω_0 becomes

$$\frac{S(0,0,\omega)}{S(0,0,\omega_0)}\simeq1+\frac{1}{18}\left(-1+16\alpha^3-24\alpha^4+8\alpha^6\right)\Delta^2(\omega) \tag{11}$$

Again, solving the corresponding second-order polynomial for a 3-dB variation, that is equating this ratio to 1/2, leads to the following 3-dB bandwidth expression

$$B=\frac{3c_0}{\pi R\sqrt{\varepsilon_r}}\frac{1}{\sqrt{1-16\alpha^3+24\alpha^4-8\alpha^6}} \tag{12}$$

As can be noticed from (12), the gain bandwidth is a function of the ring relative radius (defined by α).

Let us now determine its optimal value for wideband operation by forcing to zero the derivative of the relative bandwidth with respect to α :

$$\frac{dB}{d\alpha}=-\frac{3}{\pi R\sqrt{\varepsilon}}\frac{-48\alpha^2+96\alpha^3-48\alpha^5}{\left(\sqrt{1-16\alpha^3+24\alpha^4-8\alpha^6}\right)^3} \tag{13}$$

Solving $dB/d\alpha=0$ leads to three solutions: α =1, α =-1.6180, and α=0.6180, the only physical being the third one. For this optimal parameter value, the absolute bandwidth becomes

$$B=\frac{3c_0}{\sqrt{\varepsilon_r}\pi R}1.8944\,. \tag{14}$$

Comparing this last result with the equation (8), the bandwidth increment factor is estimated to be equal to 1.8944. From a physical point of view, the gain degradation can be reduced through the minimization of the phase error on the aperture. Since this error is proportional to the distance between the radiating elements and the feed point, placing the ring at an intermediate position on the circular antenna aperture minimizes the average error.

III. PRACTICAL IMPLEMENTATION OF A LINE-FED CP-RLSA

A. Design and Optimization

To illustrate the bandwidth improvement provided by the corporate-feed network in circular apertures, we present here the design of a 260 mm-diameter CF-RLSA based on conventional PCB technology at 29 GHz implementing an RHCP aperture field with uniform amplitude. We will first

discuss the design of the corporate-feed network, then describe the adopted optimization procedure, and finally compare the simulated patterns of the CF-RLSA with a reference optimized RLSA.

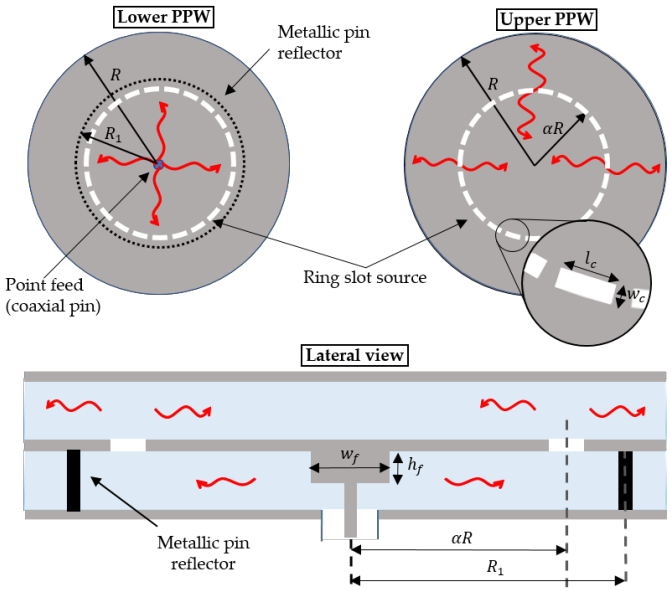

Fig. 2. Corporate-feed network implemented in PCB technology: (top left) lower PPW, (top right) upper PPW, and (bottom) lateral view.

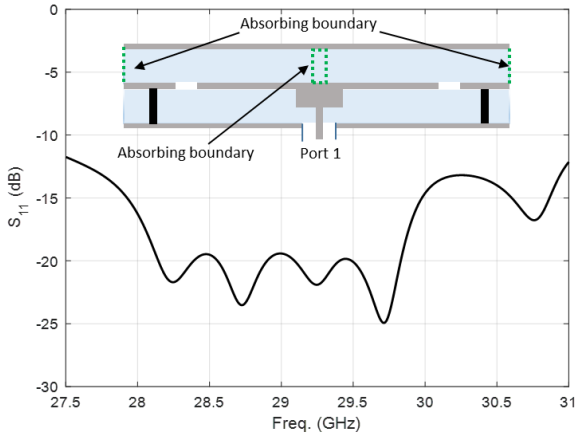

Fig. 3. Simulated reflection coefficient of the circular pillbox transition

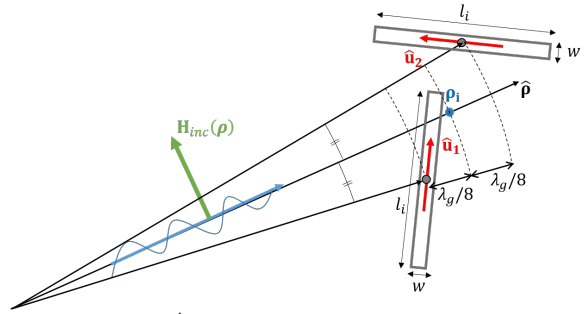

Fig. 4. Geometry of the i[th] slot pair, radiating a right-handed circular polarized field when illuminated by an outward propagating incident field $\mathbf{H}_{inc}$.

1) *Corporate feed network* : In order to realize the circular in-phase feeding of the aperture, a circular pillbox transition architecture is employed. As illustrated in Fig. 2, the antenna is made of two 1.575 mm thick Rogers RT Duroid 5880 substrates ($\varepsilon_r = 2.2$, $\tan\delta = 0.0009$) forming a stack-up of two PPWs. These substrates were chosen for their low dissipation factor, which is a critical parameter to achieving high radiation efficiency with large antennas. The lower PPW can be seen as a power distribution layer, in which a coaxial pin inserted at the center excites an outward radially propagating TEM wave. This wave is then transmitted to the upper layer thanks to the combination of a circular reflector of radius R_1 made of closely-spaced metalized via-holes and coupling slots etched in the middle metallic plane. In the upper layer, these coupling slots excite two waves propagating in opposite directions, that is toward the center and the edge.

The circular transition geometry was first optimized separately. We are dealing here with a uniform amplitude aperture field. Therefore a compromise has to be found between the optimal slot ring radius derived in section II-B (α=0.618) and the need to uniformly radiate the power on the antenna surface ($\alpha = 1/\sqrt{2} \simeq 0.707$ to have the same area for the inner and outer antenna regions). Since the two values are close to each other, the prototype transition was optimized around the second value to avoid gain degradation while maintaining a good bandwidth increment (smaller than the theoretical maximal value of 89%), and targeting minimal reflection losses over a wide frequency band. The resulting transition is made of 156 slots positioned at a radius equal to $\alpha R = (0.698)R = 90.7$ mm from the center. Evaluating (12) with this value shows that a 74% bandwidth improvement can be expected compared to the conventional RLSA (). The final parameters of the transition were found via a full-wave optimization (Ansys HFSS), leading to $R_1 = 94.45$ mm, $l_c = 3.15$ mm, and $w_c = 0.35$ mm. Finally, a partial-height metallic cylinder ($w_f = 2.7$ mm, $h_f = 0.8$ mm) was added to ensure a proper transition from the coaxial feed to the lower PPW. The simulated reflection coefficients at the coaxial feed point are illustrated in Fig. 3. As depicted, for this simulation two cylindrical absorbing boundaries were added in the upper PPW to avoid reflections toward the feed, one in the center and a second one at the outer edge. The simulated S_{11} is lower than -10 dB in the entire 27.5-31 GHz band and remains below -15 dB from 28 to 30 GHz.

2) *Slot Distribution Optimization*: The radiating slot distribution on the upper metallic layer was optimized using an in-house fast numerical tool [24], [25] along with an iterative procedure from [9]. We will briefly present here the optimization method while highlighting the modifications that were adopted for this circularly feed aperture, if necessary further details can be found in [9] for the overall procedure. Let us first consider a pair of slots positioned on top of the PPW at ρ_i radiating a circularly polarized field when illuminated by an incident field propagating along the radial vector $\boldsymbol{\rho}$, as depicted in Fig. 4. The two slots have identical dimensions l_i, w and are oriented along $\hat{\mathbf{u}}_1$ and $\hat{\mathbf{u}}_2$, respectively. In addition, they are slightly shifted along the radial axis $\hat{\boldsymbol{\rho}}$ to avoid overlaps. In this configuration, if the orthogonality of the slot's equivalent magnetic moments is imposed ($\hat{\mathbf{u}}_1 \cdot \hat{\mathbf{u}}_2 = 0$), a circular

polarization is produced at the design frequency, for which a radial distance of $2\lambda_g/8=\lambda/4$ separates the slot centers.

Such a pair of slots constitutes an elementary radiating element of the aperture. In practice, a numerical evaluation of the dipole moment of each slot is performed, then the moment of the pair is obtained with an in-house Method of Moment (MoM) [24],[25] as $\mathbf{M}(\boldsymbol{\rho}_i)=\mathbf{M}_1(\boldsymbol{\rho}_i)+\mathbf{M}_2(\boldsymbol{\rho}_i)$, where $\mathbf{M}_1(\boldsymbol{\rho}_i)=M_1\hat{\mathbf{u}}_1$ and $\mathbf{M}_2(\boldsymbol{\rho}_i)=M_2\hat{\mathbf{u}}_2$ designate the dipole moments of each slot. The optimization procedure consists in determining the positions $\boldsymbol{\rho}_i$ and lengths l_i such that a given target moment distribution can be realized on the aperture. For RH-CP antennas, the target aperture distribution is written as $\mathbf{M}^t(\boldsymbol{\rho}_i)=A(\rho)\hat{\mathbf{u}}_{RH}$, where $A(\rho)$ represents the radial amplitude distribution and $\hat{\mathbf{u}}_{RH}$ is the normalized right-handed polarization vector, given by:

$$\hat{\mathbf{u}}_{RH}=\frac{\hat{\mathbf{x}}-j\hat{\mathbf{y}}}{\sqrt{2}}. \tag{15}$$

Following [9], a complex fitness function can be defined as:

$$F(\boldsymbol{\rho}_i)=\frac{\dfrac{\mathbf{M}(\boldsymbol{\rho}_i)\cdot(\hat{\mathbf{u}}_{RH})^*}{\bar{M}}}{\dfrac{A(\boldsymbol{\rho}_i)}{\bar{A}}}, \tag{16}$$

where

$$\begin{aligned}\bar{A}&=\frac{1}{N_c}\sum_{n=1}^{N}\left|A(\boldsymbol{\rho}_i)\right|\\ \bar{M}&=\frac{1}{N_c}\sum_{n=1}^{N}\left|\hat{\mathbf{u}}_{RH}\cdot\mathbf{M}(\boldsymbol{\rho}_i)\right|\end{aligned} \tag{17}$$

are the average target and implemented dipole moment amplitude over N slot pairs. The amplitude of F is proportional to the local amplitude error, while its argument is directly the phase error.

While the slot length correction law is the same as the one presented in [9], a modified position correction law has been introduced to take into account the double nature of the incident field (outward and inward waves).

The slot length and position of the i-th pair is then be adjusted at each optimization step (s+1) based on the fitness function evaluation at step (s) by:

$$l_i^{(s+1)}=l_i^{(s)}+l_i^{(s)}\chi_l\left(1-\left|F^{(s)}(\boldsymbol{\rho}_i)\right|\sqrt{\eta_{so}^{(s)}}\right), \tag{18}$$

and

$$\rho_i^{(s+1)}=\begin{cases}\rho_i^{(s)}+\chi_\rho\dfrac{Arg\left\{F^{(s)}(\boldsymbol{\rho}_i)\right\}}{k_d} & \text{if } \rho_i>\alpha R\\ \rho_i^{(s)}-\chi_\rho\dfrac{Arg\left\{F^{(s)}(\boldsymbol{\rho}_i)\right\}}{k_d} & \text{if } \rho_i<\alpha R\end{cases} \tag{19}$$

where χ_l and χ_p are used to adjust the correction strength, typically $\chi_l=\chi_l=0.5$, In addition, the antenna spillover efficiency η_{so} is also computed at each iteration to ensure that the optimization loop runs until nearly all the accepted power at the feed is effectively radiated. It is defined as:

$$\eta_{so}=\frac{P_{acc}-P_{so}}{P_{acc}} \tag{20}$$

where P_{acc} is the power accepted by the antenna at the feeding port, whereas P_{so} is the total power trapped in the PPW beyond the slots distribution. This latter quantity η_{so} is obtained by the MoM code, when $\eta_{so}=1$ all the power injected by the feeder is radiated by the slots. The loop is repeated until η_{so} is stabilized around a sufficient value, and the average aperture distribution error ε_Δ given by (21) is sufficiently small.

$$\varepsilon_\Delta=\frac{1}{N}\sum_{n=1}^{N}\left|\hat{\mathbf{u}}_{RH}\cdot\mathbf{M}(\boldsymbol{\rho}_i)-\frac{A(\boldsymbol{\rho}_i)}{\bar{A}}\right| \tag{21}$$

For all iterations, interpolation functions were used for F, l_i, and ρ_i to improve the stability of the optimization and reduce the number of parameters. Therefore, l_i and ρ_i were indirectly adjusted via a reduced number of control points, as thoroughly described in [9].

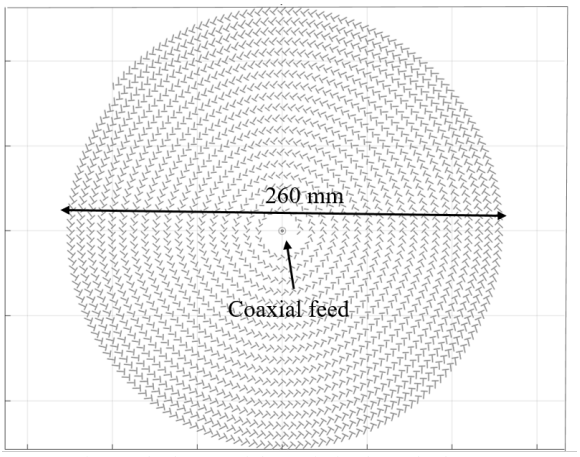

Fig. 5. The layout of the optimized standard RLSA

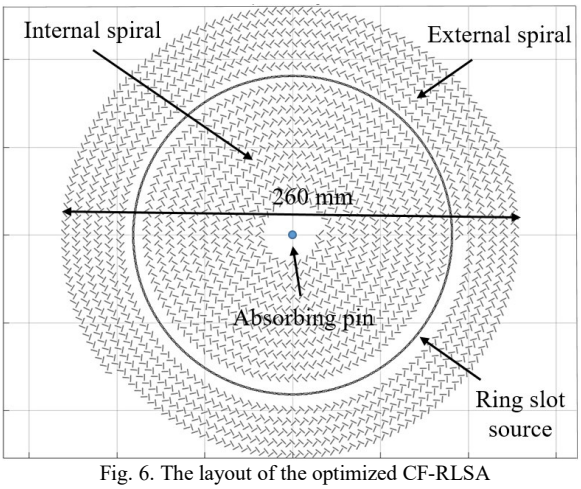

Fig. 6. The layout of the optimized CF-RLSA

For comparison purposes, a standard RLSA printed on a single layer of Rogers 5880 substrate of thickness 1.575 mm with a radius of 130 mm radius was firstly designed using the optimization method. The antenna layout is depicted in Fig. 5. The radiating aperture is composed of a total of 1842 slots of width w = 0.25 mm and lengths ranging from 2.5 mm to 4 mm. For such a center-fed aperture, it is well established that a spiral distribution of slot pairs individually radiating a circularly polarized field produces a circularly polarized broadside beam in the far-field [2]. For a line-fed aperture, however, the center radiating area is fed by an inward propagating wave, the spiral orientation should therefore be reversed to obtain a similar far-field pattern. As a consequence, the CF-RLSA is composed of two inversely rotating spirals, as illustrated in Fig. 6.

In comparison with the standard RLSA optimization, the objective field, the fitting function, and the efficiency remain the same. However, the problem arises from the inward wave excited by the annular feed, which after reaching the antenna center becomes an additional outward wave causing both unwanted additional radiation and a stationary wave in the antenna inner area as shown in Fig. 7(a). This latter aspect can deeply affect the stability of the optimization method because, as shown in Fig. 7(c), in some positions the incident field on the radiating slots can be weak or null. To deal with this problem, an absorbing pin was mathematically added at the center of the upper PPW in our numerical design tool (Figs. 7(b) and (c)), despite such a configuration does not correspond to a physically realizable antenna. Doing so leads to smooth field amplitudes, however, part of the energy will be dissipated in the pin, lowering the efficiency. Therefore, the optimization procedure ends when the efficiency becomes close to one, meaning that both the outer and the inward waves are completely radiated in the space by the slots before reaching the antenna edge and the absorbing pin, respectively. Once this configuration is reached, the absorbing pin can be safely removed to obtain a realistic design.

The starting point of the optimization is defined as follows. All slots have the same length l_0 = 2 mm and width w_0 = 0.25 mm. They are positioned along regularly sampled internal and external spiral arms with a fixed spacing dS of 4.5 mm, which is slightly lower than $\lambda_0/2$ at the design frequency of 29 GHz. The evolutions of the average aperture distribution error ε_Δ and spillover efficiency η_{so} during the optimization procedure are illustrated in Fig. 8. The spillover efficiency very rapidly stabilizes itself around its final value of 0.91, while about 20 iterations are required for the average aperture error to reach a minimum value of 0.22. In the end, the radiating aperture consists of 807 slots in the internal spiral and 879 slots in the external spiral, with lengths ranging from 3.6 to 3.9 mm.

The phase and magnitude of the fitness function F_i at the end of the optimization are depicted in Fig. 9. The magnitude of F_i is close to 1 for most slot pairs, with a lower value at the outer edge of the antenna, caused by the trade-off between achieving uniform illumination while minimizing spillover loss. The constant phase value of F_i reflects the in-phase radiation of all slot pairs. In terms of computing resources required for the optimization, a single iteration step takes about 25 minutes on an office laptop equipped with an Intel i5 7300U processor combined with 8 GB of RAM.

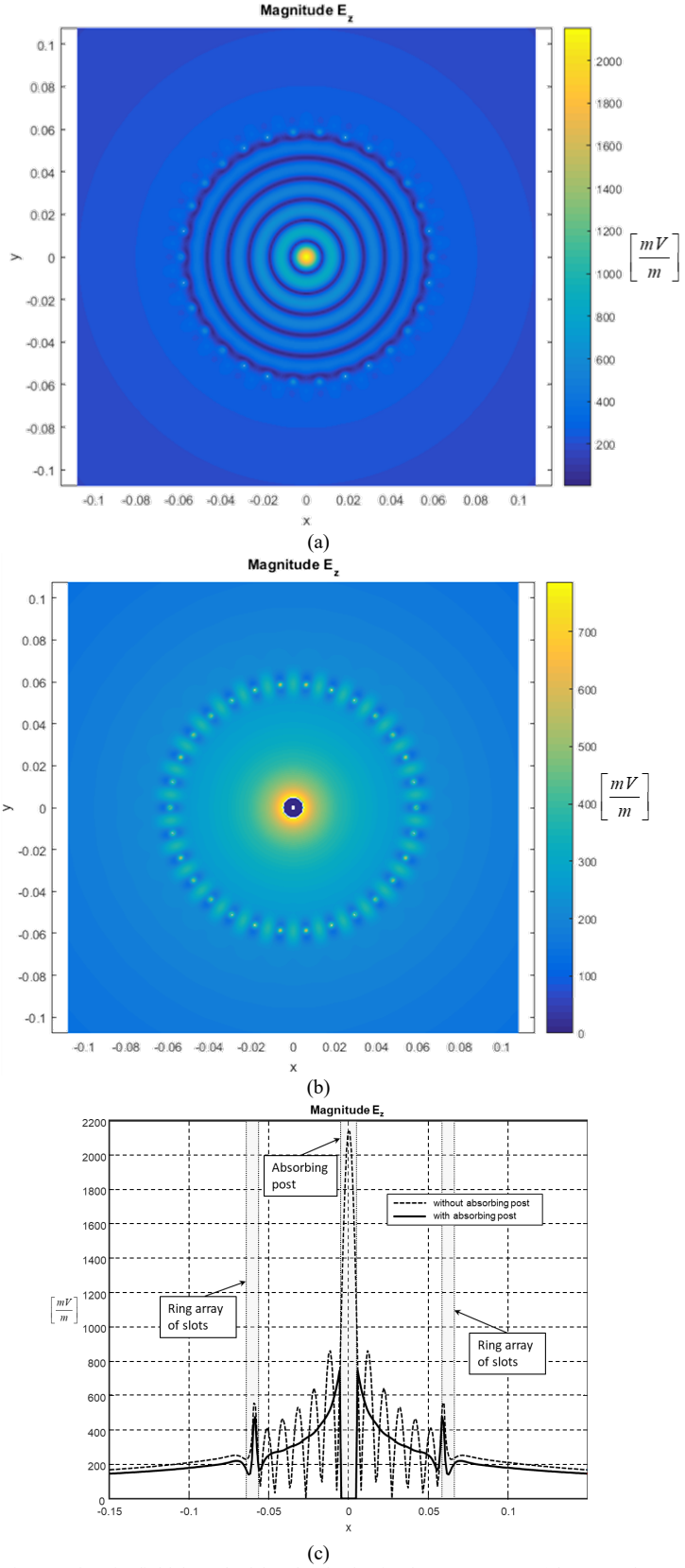

Fig. 7. Electric field launched by the feeder in the upper PPW (absence of radiating slots). (a) Stationary wave presence in the internal area. (b) Effect of the introduction of the absorbing central post. (c) Comparison of the radiation patterns in the horizontal cut-plane with and without the central absorbing pin.

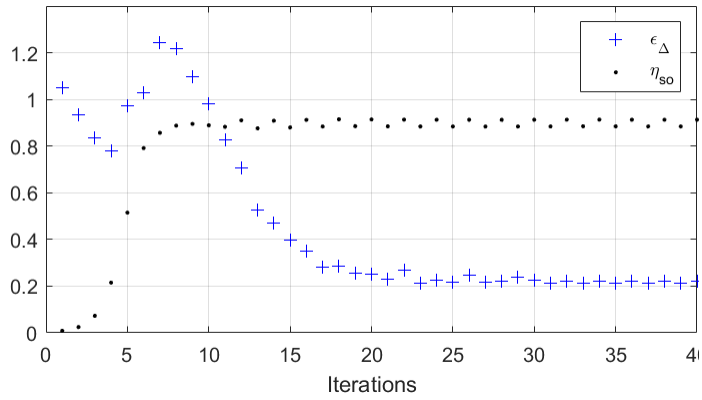

Fig. 8. Evolution of the average aperture distribution error ε_Δ and spillover efficiency η_{so} during the optimization procedure

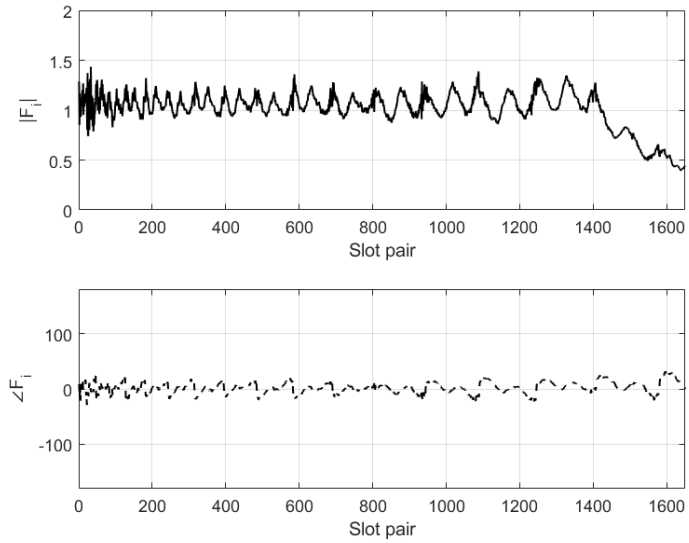

Fig. 9. The amplitude and phase of the fitness function at the end of the optimization procedure

B. Simulation results

Both RLSA and CF-RLSA far-field patterns were computed. The complete simulation was performed with the commercial software Ansys HFSS, taking into account the finite size of the substrate. The simulated gains are illustrated in Figs. 10 and 11, respectively. The RLSA exhibits a broadside 36.8 dBi gain at the design frequency of 29 GHz, however, this gain rapidly degrades with frequency, reaching about 27 dBi at 28 GHz and 30 GHz. In comparison, the CF-RLSA shows a very stable radiation pattern over a larger bandwidth. The obtained radiation efficiencies at the central frequency for the RLSA and the CF-RLSA are 86% and 82%, respectively. The difference could be explained by the dielectric and ohmic losses in the propagation through the corporate feeder.

While a slightly lower gain of 35.7 dBi is achieved at the center frequency, a gain higher than 27 dBi is maintained from 27 to 32 GHz. This simulation result clearly demonstrates the impact of the reduced phased error on the aperture provided by the corporate feed.

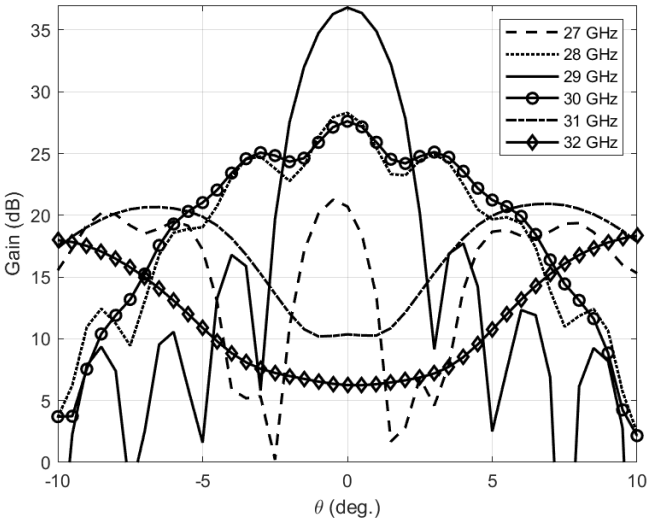

Fig. 10. The simulated gain pattern of the optimized RLSA

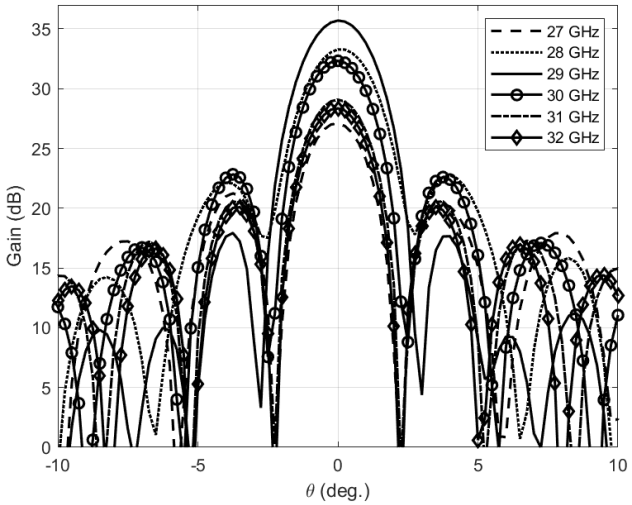

Fig. 11. The simulated gain pattern of the optimized CF-RLSA

C. Fabrication and measurements

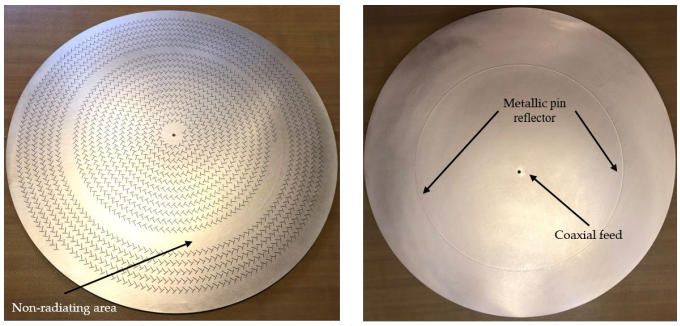

Fig. 12. Realized CF-RLSA antenna: (left) Top-view and (right) bottom view

The optimized CF-RLSA was realized using standard PCB technology. The prototype is depicted in Fig. 12. On the upper layer, one can see the two spirals with opposite rotation directions, as well as the non-radiating area located above the feed. On the opposite side, the coaxial feed point, as well as the metallic pins for the pillbox transition, are visible. The measured and simulated gain patterns are compared in Fig. 13 at frequencies between 27 and 32 GHz. To ensure the readability of the results, the graphs have been limited to the [-30°,30°] angular range. The complete scan at the design frequency for measurements is reported in Fig. 14.

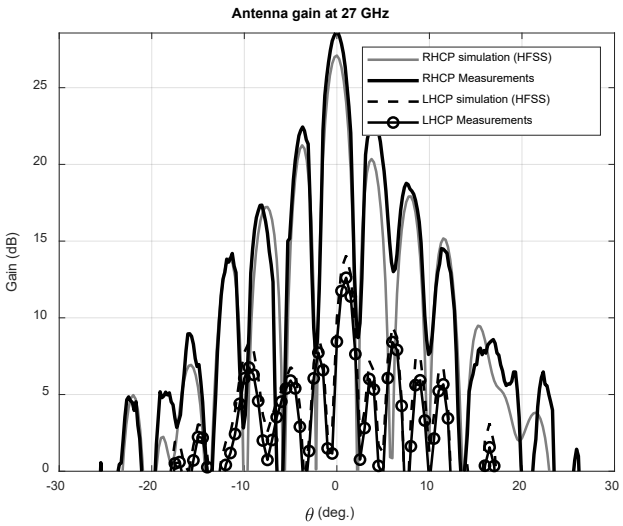

(a)

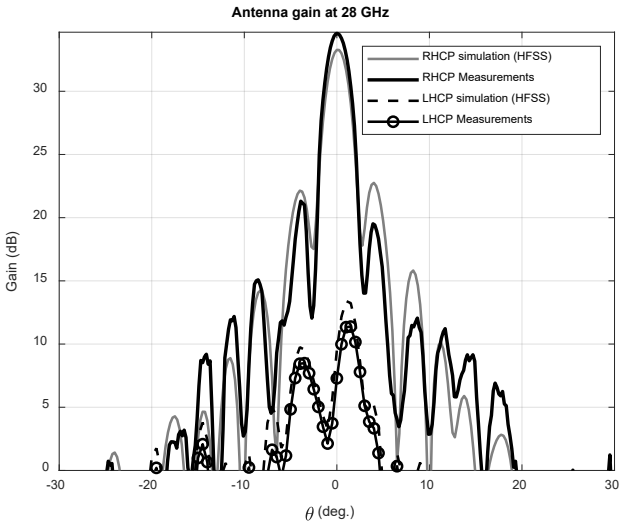

(b)

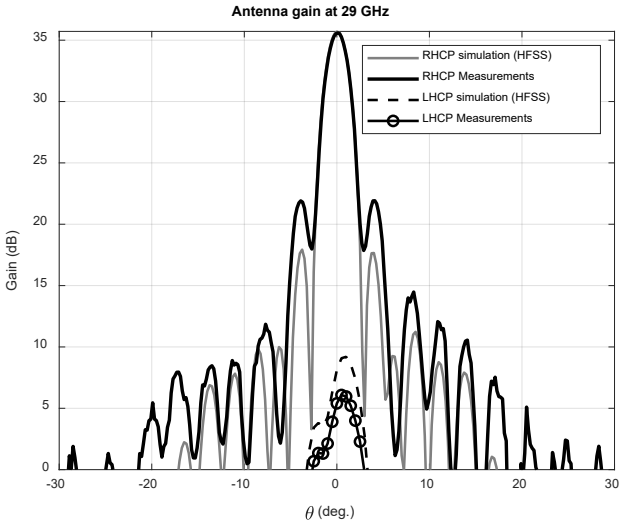

(c)

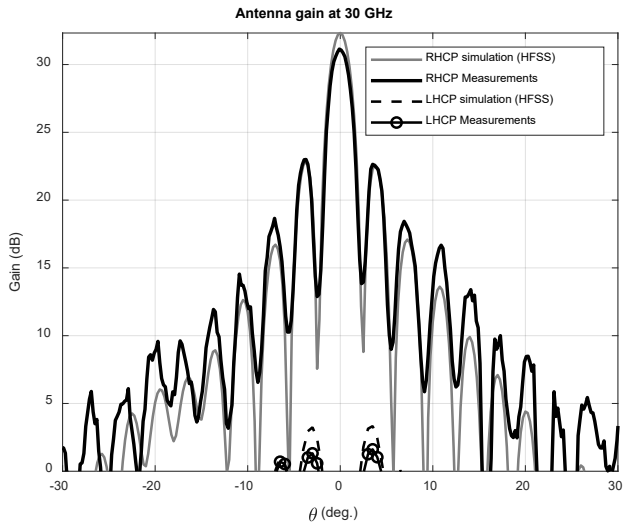

(d)

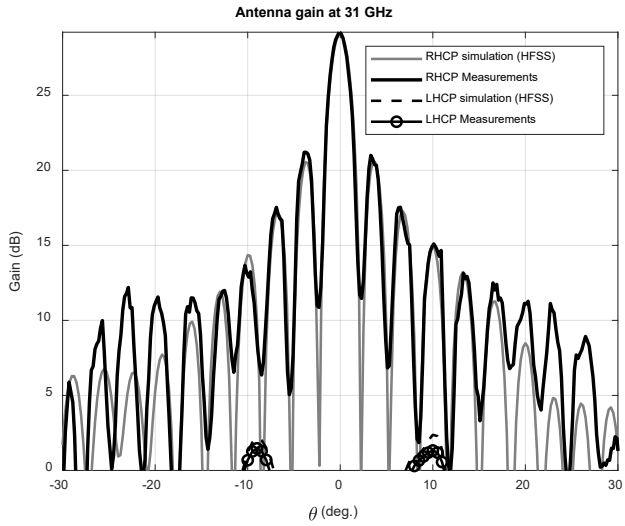

(e)

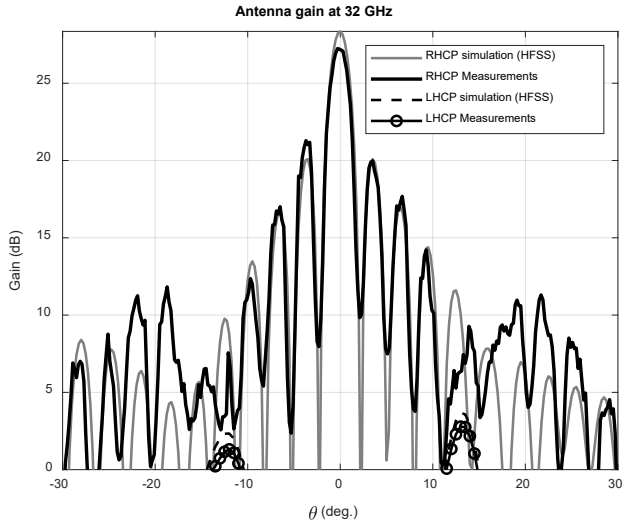

(f)

Fig. 13. Measured and simulated gain patterns (ϕ= 0 deg.) at (a) 27, (b) 28, (c) 29, (d) 30, (e) 31 and (f) 32 GHz.

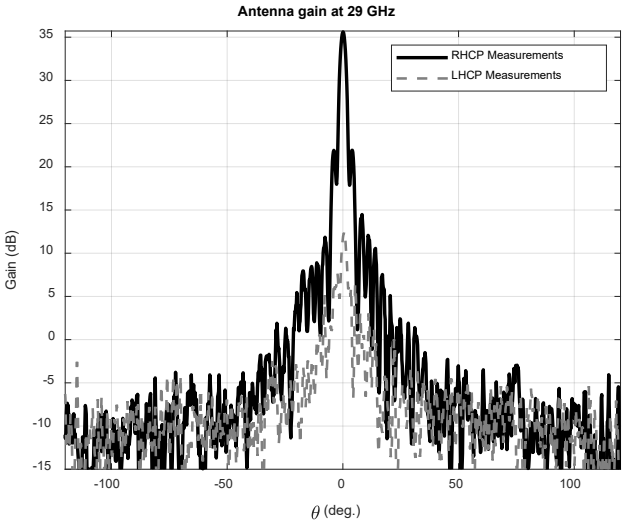

Fig. 14. Measured gain pattern (ϕ= 0 deg.) at 29 GHz.

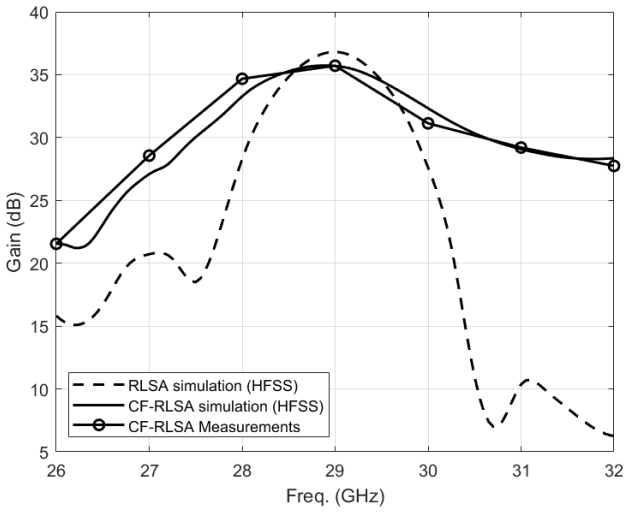

Fig. 15. Measured and simulated gain versus frequency for both RLSA and CF-RLSA.

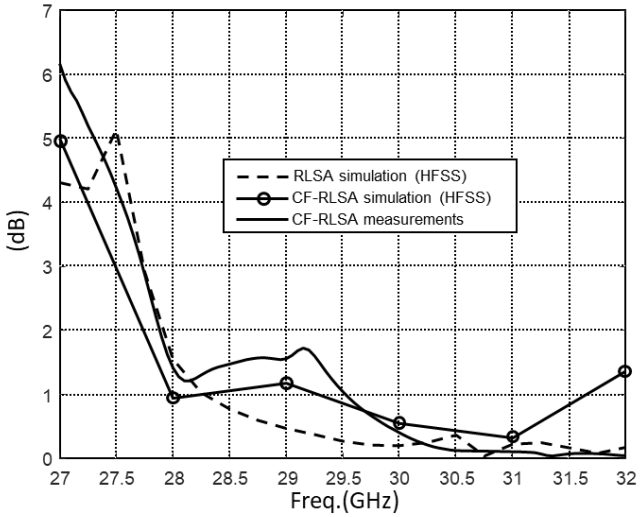

Fig. 16. Measured and simulated broadside axial ratio for both RLSA and CF-RLSA.

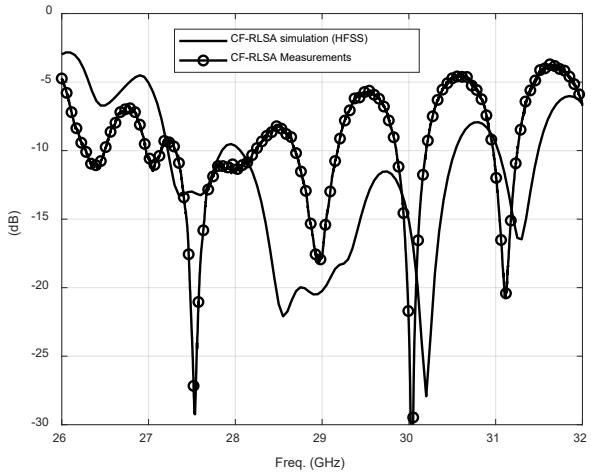

Fig. 17. Measured and simulated reflection coefficient of CF-RLSA

First of all, a stable broadside beam with right-handed circular polarization was measured in the band 27-32 GHz, with side lobes level (SLL) reaching a minimum of -14 dB at 29 GHz and a maximum of -6 dB at 27 GHz. The cross-polarized left-handed radiation level is 10 dB below the co-polarization at 27 GHz and remains 20 dB lower for all other frequencies. Finally, an overall good agreement between simulations and measurements was observed.

The realized gain for both simulated and measured CF-RLSA, as well as RLSA, are given in Fig. 15, while the axial ratio is reported in Fig.16. As already illustrated by Figs. 9 and 10, the corporate feeding technique provides a much less dispersive radiation pattern, as clearly visible in this gain vs. frequency diagram. Simulated and measured gains of the CF-RLSA are in good agreement, despite a slight shift toward lower frequencies in measurements. A maximum gain of 35.7 dBi was measured at 29 GHz, as expected in simulations. A 3-dB gain bandwidth of about 2 GHz was measured, as compared to 1.97 GHz in simulations. On the other hand, the simulated RLSA exhibits a slightly higher gain of 36.8 dBi at 29 GHz with a 3 dB gain bandwidth of 1.2 GHz. The estimated improvement of gain bandwidth achieved by the ring feed is therefore 67%, closely approaching the estimated 70% in Sec. III-A1.

Finally, the measured and simulated reflection coefficients S_{11} at the input of both antennas are represented in Fig. 17. In the simulation, a reflection coefficient greater than 10 dB between 28.16 and 30.57 GHz was obtained, however, a degraded reflection was observed in measurements. This discrepancy can be explained by fabrication constraints related to the coaxial transition, which unfortunately impacted the measured response.

The performances of the proposed antenna are given in Table 2 and compared with existing RLSA designs specifically addressing the bandwidth limitation. The reference RLSA design from this paper is also included. The comparison is based on the real (or effective) permittivity of the radiating layer, manufacturing technology, realized gain, 3-dB gain fractional bandwidth (FBW), aperture efficiency, and gain-bandwidth product (GFBW) over aperture radius (in wavelength) multiplied by $\sqrt{\varepsilon_r}$ (GFBW$\sqrt{\varepsilon_r}\lambda_0$/R). Contrary to GFBW, this last figure-of-merit does not depend on the antenna

radius (in free-space wavelengths) nor substrate permittivity, which allows for comparing the antenna performances in terms of designs, materials aside. Indeed, it can be easily shown that from (8) and (14) GFBW is proportional to $R/(\lambda_0\sqrt{\varepsilon_r})$. Finally, the aperture efficiency of the CF-RLSA is estimated by removing the simulated radiation efficiency from the measured gain, which is very close to the simulated one, and for reference [18] the intermediate permittivity of 1.2 was considered in the calculation.

Ref.	Freq. (GHz)	ε_r	Tech.	Gain (dBi)	FBW (%)	η_{ap} (%)	GFBW$\sqrt{\varepsilon_r}\lambda_0$/R
RLSA[1]	29	2.2	PCB	36.8	4.1	89	23.2
This work	**29**	**2.2**	**PCB**	**35.7**	**6.9**	**73**	**30.3**
[17][1]	19.4	1.41	Hybrid	31.2	6.2	62	12.5
[18]	11	1-1.4	Hybrid	27.3	27.6	28	22.1
[21]	11.85	1.59	Metal	33.7	6.7	42	16.7

Table 1. Comparison of the proposed CF-RLSA design to the state-of-the-art solutions.

While using a standard manufacturing process (PCB), the proposed antenna offers the greatest GFBW$\sqrt{\varepsilon_r}\lambda_0$/R (30.3, versus 22.1 for [18]), which shows the significant impact on bandwidth improvement of the corporate feeding while maintaining a good aperture efficiency (73%).

IV. Conclusion

In this paper, we demonstrate the benefit of corporate-feed networks for RLSAs in terms of gain stability and operational bandwidth compared to classical designs. In particular, a 130 mm radius CF-RLSA incorporating a circular pillbox transition in Ka-band was designed, fabricated with low-cost PCB technology, and characterized. A 67% bandwidth increase was obtained with respect to conventional RLSA designs. This work could be of interest for achieving even wider bandwidths and higher gains with low-cost flat radiating panels for a variety of applications, such as satellite links or next-generation communication networks in the millimeter-wave range and beyond.

References

[1] F. Goebels and K. Kelly, "Arbitrary polarization from annular slot planar antennas," *IEEE Transactions on Antennas and Propagation*, vol. 9, pp. 342–349, 1961.

[2] M. Takahashi, J. Takada, M. Ando, and N. Goto, "A slot design for uniform aperture field distribution in single-layered radial line slot antennas," *IEEE Transactions on Antennas and Propagation*, vol. 39, no. 7, pp. 954–959, July 1991USA.

[3] M. Ando, K. Sakurai, N. Goto, K. Arimura, and Y. Ito, "A radial line slot antenna for 12 GHz satellite tv reception," *IEEE Transactions on Antennas and Propagation*, vol. 33, no. 12, pp. 1347–1353, December 1985.

[4] M. Takahashi, M. Ando, N. Goto, Y. Numano, M. Suzuki, Y. Okazaki, and T. Yoshimoto, "Dual circularly polarized radial line slot antennas," *IEEE Transactions on Antennas and Propagation*, vol. 43, no. 8, pp. 874–876, 1995.

[5] J. Takada, M. Ando, and N. Goto, "A reflection canceling slot set in a linearly polarized radial line slot antenna," *IEEE Transactions on Antennas and Propagation*, vol. 40, no. 4, pp. 433–438, 1992.

[6] A. Mazzinghi, M. Albani, and A. Freni, "Double-spiral linearly polarized RLSA," *IEEE Transactions on Antennas and Propagation*, vol. 62, no. 9, pp. 4900–4903, 2014.

[7] V. Pla, A. Valero-Nogueira, J. Herranz, E. Alfonso, and V. Rodrigo, "Dual linearly polarized single-layer radial-line slot-array antenna," *IEEE Antennas and Wireless Propagation Letters*, vol. 5, pp. 120–122, 2006.

[8] T. Nguyen, H. Ueda, J. Hirokawa, and M. Ando, "A radial line slot antenna for an elliptical beam," *IEEE Transactions on Antennas and Propagation*, vol. 60, no. 12, pp. 5531–5537, 2012.

[9] M. Albani, A. Mazzinghi, and A. Freni, "Automatic design of CP-RLSA antennas," *IEEE Transactions on Antennas and Propagation*, vol. 60, no. 12, pp. 5538–5547, 2012.

[10] M. Sierra-Castaner, M. Sierra-Perez, M. Vera-Isasa, and J. Fernandez-Jambrina, "Low-cost monopulse radial line slot antenna," *IEEE Transactions on Antennas and Propagation*, vol. 51, no. 2, pp. 256–263, 2003.

[11] J. I. Herranz, A. Valero-Nogueira, F. Vico, and V. M. Rodrigo, "Optimization of beam-tilted linearly polarized radial-line slot-array antennas," *IEEE Antennas and Wireless Propagation Letters*, vol. 9, pp. 1165–1168, 2010.

[12] M. Ettorre, M. Casaletti, G. Valerio, R. Sauleau, L. Le Coq, S. C. Pavone, and M. Albani, "On the near-field shaping and focusing capability of a radial line slot array," *IEEE Transactions on Antennas and Propagation*, vol. 62, no. 4, pp. 1991–1999, 2014.

[13] A. Mazzinghi, M. Balma, D. Devona, G. Guarnieri, G. Mauriello, M. Albani, and A. Freni, "Large depth of field pseudo-bessel beam generation with a RLSA antenna," *IEEE Transactions on Antennas and Propagation*, vol. 62, no. 8, pp. 3911–3919, 2014.

[14] A. Mazzinghi, A. Freni, and M. Albani, "Influence of the finite slot thickness on RLSA antenna design," *IEEE Transactions on Antennas and Propagation*, vol. 58, no. 1, pp. 215–218, 2010.

[15] M. Albani, A. Mazzinghi, and A. Freni, "Rigorous MoM analysis of finite conductivity effects in RLSA antennas," *IEEE Transactions on Antennas and Propagation*, vol. 59, no. 11, pp. 4023–4032, 2011.

[16] T. Salmeron-Ruiz, T. Díez-Ricondo, and M. Sierra-Castañer, "An optimization procedure for radial line slot antennas with arbitrary pattern,"in *The 8th European Conference on Antennas and Propagation (EuCAP 2014)*, 2014, pp. 1793–1796.

[17] N. Y. Koli, M. U. Afzal, K. P. Esselle and M. Z. Islam, "Comparison Between Fully and Partially Filled Dielectric Materials on the Waveguide of Circularly Polarised Radial Line Slot Array Antennas," 2020 International Workshop on Antenna Technology (iWAT), 2020, pp. 1-3.

[18] M. N. Y. Koli, M. U. Afzal and K. P. Esselle, "Significant Bandwidth Enhancement of Radial-Line Slot Array Antennas Using a Radially Nonuniform TEM Waveguide," in *IEEE Transactions on Antennas and Propagation*, vol. 69, no. 6, pp. 3193-3203, June 2021.

[19] N. Y. Koli, M. U. Afzal, K. P. Esselle and M. Z. Islam, "Comparison Between Fully and Partially Filled Dielectric Materials on the Waveguide of Circularly Polarised Radial Line Slot Array Antennas," 2020 International Workshop on Antenna Technology (iWAT), 2020, pp. 1-3.

[20] T. P. C. LTD, "Composite structure radial line slot antenna," Patent 0 097 605, April, 1991.

[21] T. Yamamoto, M. Takahashi, M. Ando and N. Goto, "Measured performances of a wide band radial line slot antenna," Proceedings of *IEEE Antennas and Propagation Society International Symposium and URSI National Radio Science Meeting*, 1994, pp. 2204-2207 vol.3, doi: 10.1109/APS.1994.408046.

[22] K. Tekkouk, M. Ettorre, E. Gandini, and R. Sauleau, "Multibeam pillbox antenna with low sidelobe level and high-beam crossover in SIW technology using the split aperture decoupling method," *IEEE Transactions on Antennas and Propagation*, vol. 63, no. 11, pp. 5209–5215, 2015.

[23] M. Ettorre, R. Sauleau, and L. Le Coq, "Multi-beam multi-layer leakywave SIW pillbox antenna for millimeter-wave applications," *IEEE Transactions on Antennas and Propagation*, vol. 59, no. 4, pp. 1093–1100, 2011.

[24] M. Casaletti, G. Valerio, J. Seljan, M. Ettorre, and R. Sauleau, "A full-wave hybrid method for the analysis of multilayered SIW-based antennas," *IEEE Transactions on Antennas and Propagation*, vol. 61.

[25] M. Casaletti, G. Valerio, R. Sauleau, and M. Albani, "Mode-matching analysis of lossy SIW devices," *IEEE Transactions on Microwave Theory and Techniques*, vol. 64, no. 12, pp. 4126–4137, 2016.